

Mapping of Optical Pathlength of Human Adult Head at Multi-Wavelengths in Near Infrared Spectroscopy

Akihisa Katagiri, Ippeita Dan, Daisuke Tuzuki, Masako Okamoto, Noriaki Yokose, Kouji Igarashi, Tatsuya Hoshino, Tokuo Fujiwara, Youichi Katayama, Yui Yamaguchi, and Kaoru Sakatani

Abstract Measurement of multichannel continuous-wave near-infrared spectroscopy (CW-NIRS) is dependent on the modified Beer-Lambert law, which includes optical pathlength (PL) as an essential parameter. PLs are known to differ across different head regions and different individuals, but the distribution of PLs for the whole head has not been evaluated so far. Thus, using time-resolved near-infrared spectroscopy (TR-NIRS), we measured the optical characteristics including PL, scattering coefficients (μ'_s), and absorption coefficients (μ_a) at three wavelengths (760, 800, 830 nm). Then, we constructed maps of these parameters on the subjects' head surface. While the PLs in nearby channels are similar, they differ depending on the regions of the head. The PLs in the region above the Sylvian fissure tended to be shorter than those in the other regions at all of the wavelengths. The difference in the distribution of PLs may be attributed to differences in tissue absorption and scattering properties. The current study suggests the importance of considering PL differences in interpreting functional data obtained by CW-NIRS.

1 Introduction

Multichannel continuous-wave near-infrared spectroscopy (CW-NIRS), also known as functional NIRS (fNIRS), or Optical topography (OT), is an emerging neuroimaging technique that allows the noninvasive monitoring of hemodynamic changes associated with human brain activity [1]. CW-NIRS has several advantages with respect to other neuroimaging methods: it is more tolerant of physical movements, allows more freedom in choice of experimental settings and is less expensive. Thus, CW-NIRS has been applied in various

K. Sakatani (✉)

Division of Optical Brain Engineering, Department of Neurological Surgery; Division of Applied System Neuroscience, Department of Advanced Medical Science, Nihon University School of Medicine, Tokyo, 173-8610, Japan
e-mail: sakatani@med.nihon-u.ac.jp

diagnostic settings, including pre-surgery language dominance determination [2], preoperative planning of tumor removal [3], determining epileptic foci [4], monitoring rehabilitation [5], psychiatric diagnosis [6], pediatric diagnosis [7] and postoperative cerebral oxygenation monitoring [8].

Despite these merits, CW-NIRS measurement still has a technical drawback in that it measures absorbance without reference to optical pathlength (PL). Lack of this variable makes it impossible to calculate absolute, rather than relative changes of hemoglobin concentration when using the modified Beer Lambert law [9]. A recent study examining PL in foreheads, somatosensory motor and occipital regions revealed that PL varied among the regions of head and subjects [10], suggesting that the analysis can not be extended to the comparison between data from different channels. Also, data integration between different channels, which is necessary for topographic map reconstruction, is difficult to validate. This limits the potential of CW-NIRS measurement.

Thus, as a step toward solving the optical PL issue in CW-NIRS, we created a whole-head optical PL map by measuring PL at various regions of an adult head using time-resolved near-infrared spectroscopy (TR-NIRS). Using this, we assess the regional difference of the optical PL across different cortical regions, and discuss the feasibility of data integration among different channels.

2 Method

2.1 TR-NIRS System

We used a TR-NIRS system (TRS-10, Hamamatsu Photonics K.K., Japan) [11] to measure optical PL at three different wavelengths (760, 800, 830 nm) in normal adult subjects ($n = 8$). Detailed description of the apparatus and mechanism of the measurement is as previously described [12]. Briefly, the light source of the system emits a 5 MHz of light pulses at the three wavelengths from semiconductor lasers (Picosecond Light Pulser, Hamamatsu Photonics K.K., Japan). The light is guided through an illuminating optical fiber and emitted onto the scalp, traveling through the head and brain tissue. Some fraction of the light reaches a detecting optical fiber placed on the scalp 3 cm away from the illuminating optical fiber, and is guided into a photomultiplier tube (PMT, H6279-MOD, Hamamatsu Photonics K.K., Japan) to generate an electric signal. This signal is processed by constant fraction discriminators, time-to-amplitude converters, A/D converters and histogram memories. The mean PL was calculated from the observed temporal profiles of the light intensity [13]. Also, by fitting the observed temporal profiles to the photon diffusion equation [14], using a non-linear least square fitting method, we calculated the reduced scattering (μ'_s) and absorption coefficients (μ_a) at the three wavelengths.

2.2 Data Analysis

The midpoint between illuminating and detecting optical fibers defined a channel, the point where the optical properties of the underlying tissue was monitored. In a pilot study, we confirmed that the directional anisotropy of the channel placement was negligible. We selected approximately 80 evenly distributed scalp positions and marked them on a flexible mesh cap according to the 10–20 system of EEG placement [15]. We sequentially placed the channels at the scalp positions and performed TRS measurements. After each TRS measurement, the location of the fiber placement was measured by a 3D-magnetic digitizer (FASTRAK, Polhemus, Colchester, VT), and these locations were translated to segmented magnetic resonance images of each subject. In this way, we constructed a PL distribution map on the scalp. For all surface positions on the scalps of the subjects, the optical PLs were interpolated at a $1 \times 1 \times 1$ mm resolution, from the measuring points using a nearest neighbor method. For creating the PL distribution map on the cortical surface, each head surface position was projected onto the cortical surface as previously described [16].

3 Results

The spatial distribution of the optical PLs, μ_a and μ'_s for a subject is shown in Fig. 1. We used the optical properties measured at the international 10–20 positions (20 positions; summarized in Table 1) to perform statistical analysis. To assess laterality effects, zenith positions (Fz, Cz and Pz) were excluded. The remaining positions were divided into eight pairs of laterally symmetrical positions. A $2 \times 3 \times 8$ (laterality \times pathlengths \times positions) ANOVA was performed on the values for PL, μ_a and μ'_s . For PL, there was no significant main effect ($P < 0.05$) of laterality ($F_{(1,7)} = 0.4$) whereas significant main effects for pathlength ($F_{(2,14)} = 121.2$) and position ($F_{(7,49)} = 20.6$) were observed.. A significant interaction between pathlength and position ($F_{(14,98)} = 6.2$) was also detected. An ad-hoc multiple comparison revealed the following relation: $PL_{760} = PL_{800} > PL_{830}$ ($P < 0.05$, Bonferroni-corrected). Generally, differences in optical PLs among neighboring channels were rather small, but some global tendencies were observed. The PLs were the shortest in the peri-Sylvian regions located at the border between frontal and temporal regions. The regions above the temporal lobe also exhibited relatively short PLs. The longest PL was observed in the medial frontal and occipital regions. Frontal and parietal regions exhibited moderate PLs. These overall tendencies were observed at all of the wavelengths.

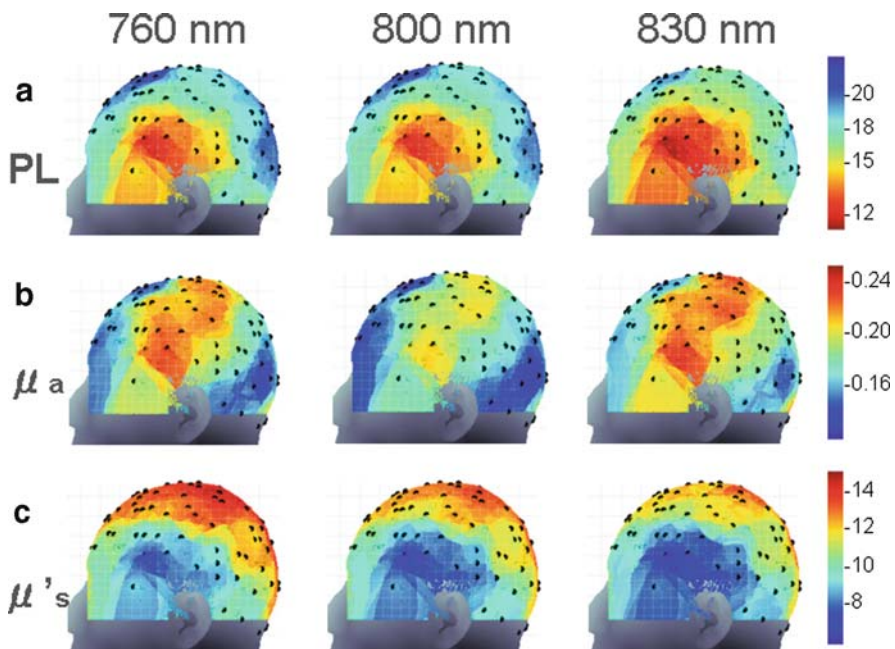


Fig. 1 **a:** Distribution of optical pathlength (PL) in a unit of cm on a scalp at 760, 800, and 830 nm. **b:** Distribution of scattering coefficients (μ_a) in a unit of cm^{-1} on a scalp at 760, 800, and 830 nm. **c:** Distribution of absorption coefficients (μ'_s) in a unit of cm^{-1} on a scalp at 760, 800, and 830 nm

While ANOVA revealed no significant main effect of laterality for μ_a ($F_{(1,7)} = 0.3$), there were significant main effects for pathlength ($F_{(2,14)} = 35.8$) and position ($F_{(7,49)} = 9.5$). Significant interaction between pathlength and position ($F_{(14,98)} = 10.3$) was also detected. Use of an ad-hoc multiple comparison revealed the following relation: $\mu_{a830} = \mu_{a760} > \mu_{a800}$ on most positions except for F4, O2, P3, P7, and P8 exhibiting $\mu_{a830} > \mu_{a760} > \mu_{a800}$ relation ($P < 0.05$, Bonferroni-corrected). Generally, μ_a was larger in the region above the central sulcus.

For μ'_s , ANOVA revealed no significant main effect of laterality ($F_{(1,7)} = 0.3$), whereas significant main effects for pathlength ($F_{(2,14)} = 29.1$) and position ($F_{(7,49)} = 6.3$) were detected. Significant interaction between pathlength and position ($F_{(14,98)} = 2.2$) was also detected, with ad-hoc multiple comparison revealing the relation: $\mu'_{s760} = \mu'_{s800} > \mu'_{s830}$ at most positions except for Fp1, F7, and P7 exhibiting only $\mu'_{s760} > \mu'_{s800}$ relation, and F8 exhibiting $\mu'_{s760} > \mu'_{s830}$ relation ($P < 0.05$, Bonferroni-corrected). Generally, μ'_s was larger in the regions above the inter-hemispherical fissure.

Table 1 Distribution of optical parameters. All values are presented as mean \pm standard deviation

Optical PL (cm)	μ_a (cm $^{-1}$)			μ'_s (cm $^{-1}$)		
	760 nm	800 nm	830 nm	760 nm	800 nm	830 nm
Fp1	22.1 \pm 4.4	22.2 \pm 4.7	21.1 \pm 4.7	0.15 \pm 0.03	0.14 \pm 0.03	0.16 \pm 0.03
Fp2	23.1 \pm 3.9	23.0 \pm 3.8	21.7 \pm 3.7	0.16 \pm 0.04	0.15 \pm 0.03	0.16 \pm 0.04
F3	21.0 \pm 4.6	21.1 \pm 4.8	19.9 \pm 4.6	0.17 \pm 0.05	0.16 \pm 0.05	0.18 \pm 0.06
F4	22.3 \pm 3.5	22.5 \pm 3.5	21.0 \pm 3.4	0.17 \pm 0.05	0.16 \pm 0.04	0.18 \pm 0.05
F7	16.1 \pm 2.0	16.4 \pm 2.5	15.6 \pm 2.3	0.23 \pm 0.07	0.21 \pm 0.06	0.23 \pm 0.07
F8	17.6 \pm 3.0	17.8 \pm 2.7	16.9 \pm 2.6	0.24 \pm 0.11	0.21 \pm 0.10	0.24 \pm 0.11
Fz	24.4 \pm 3.2	24.0 \pm 3.1	22.8 \pm 3.2	0.16 \pm 0.04	0.16 \pm 0.05	0.17 \pm 0.05
T7	17.7 \pm 3.7	17.8 \pm 3.7	17.1 \pm 3.7	0.19 \pm 0.03	0.17 \pm 0.03	0.19 \pm 0.03
T8	17.8 \pm 3.0	17.8 \pm 3.0	16.9 \pm 2.9	0.19 \pm 0.06	0.17 \pm 0.06	0.19 \pm 0.06
C3	21.0 \pm 2.4	21.0 \pm 2.3	19.9 \pm 2.2	0.21 \pm 0.05	0.19 \pm 0.05	0.21 \pm 0.05
C4	20.8 \pm 4.0	20.8 \pm 3.8	19.7 \pm 3.7	0.20 \pm 0.04	0.18 \pm 0.04	0.21 \pm 0.05
C7	21.9 \pm 4.3	21.7 \pm 4.2	20.9 \pm 4.0	0.22 \pm 0.07	0.21 \pm 0.07	0.23 \pm 0.08
P3	23.8 \pm 4.8	23.7 \pm 4.5	22.5 \pm 4.4	0.16 \pm 0.04	0.15 \pm 0.04	0.17 \pm 0.04
P4	23.3 \pm 4.4	23.3 \pm 4.3	21.9 \pm 4.3	0.16 \pm 0.03	0.15 \pm 0.03	0.16 \pm 0.03
P7	22.4 \pm 5.0	22.2 \pm 4.9	21.2 \pm 4.8	0.14 \pm 0.03	0.13 \pm 0.03	0.15 \pm 0.03
P8	22.5 \pm 3.8	22.3 \pm 3.6	21.2 \pm 3.5	0.15 \pm 0.04	0.15 \pm 0.04	0.16 \pm 0.04
Pz	22.7 \pm 3.5	22.4 \pm 3.6	21.4 \pm 3.4	0.17 \pm 0.04	0.17 \pm 0.04	0.19 \pm 0.05
O1	22.7 \pm 5.9	22.8 \pm 5.6	21.6 \pm 5.5	0.14 \pm 0.02	0.13 \pm 0.02	0.14 \pm 0.02
O2	24.1 \pm 4.2	24.0 \pm 4.1	22.8 \pm 4.0	0.15 \pm 0.03	0.14 \pm 0.03	0.16 \pm 0.04
Oz	24.4 \pm 4.5	24.1 \pm 4.4	23.1 \pm 4.4	0.14 \pm 0.03	0.13 \pm 0.03	0.15 \pm 0.03

4 Discussion

The current study extends the former study by Zhao et al. assessing optical PL distribution in the forehead, Somatosensory motor and occipital regions [10]. We broadened the region of interest to the whole head and demonstrated that optical PL varies among scalp locations, with those above the peri-Sylvian regions being the shortest and those in medial frontal and occipital regions being the longest. The inhomogenous nature of the optical PLs may be attributed to inhomogenous distribution of absorbent and tissue structures. The former is well represented by the distribution of μ_a . The observation that μ_a was smallest at 800 nm, which is the equiabsorbance point for oxygenated and deoxygenated Hbs, suggests that Hb concentration is a dominant factor in determining μ_a . Large μ_a in the region around the central sulcus likely signify a higher Hb concentration in this region, probably due to the bridging veins around the superior sagittal sinus and the Sylvian veins. In addition, the effects of the temporal muscle would play a part. On the other hand, μ'_s is expected to reflect differences in tissue properties; however, the medially-oriented larger distribution of μ'_s suggests a contribution of skull thickness. Since the current analysis did not involve elaborate segmentation of the tissues, we cannot specify which component was the most influential, and further study will be necessary to clarify the detailed aspects of tissue contribution. In addition, there was no laterality in the optical parameters tested. This finding may provide experimental support for the interhemispheric comparison of cortical activation on symmetrical regions often practiced in various CW-NIRS studies (e.g., language dominance assessment [2]).

In this study, we have presented the PL distribution on the subject's own MRI and left inter-subject integration as a future topic of study. Our intention here was to simply perform spatial normalization of the data to the standard stereotaxic brain space using transformation based on gross matching of cortical structures. However, we noted the substantial effects of non-cortical structure on PL distribution, probably due to temporal muscles and Sylvian veins. In this case, spatial normalization of the data solely based on cortical structure may be misleading, and scalp-based normalization would be more appropriate. Since there is no such method established for this, we are currently developing one.

5 Conclusion

We constructed a whole-head map for optical PL distribution. While the PLs in local vicinities are similar, they differ according to locations on the head. The difference in the distribution of PLs may be further attributed to differences in tissue absorption and scattering properties. The current study suggests the importance of considering PL differences in interpreting functional data obtained by CW-NIRS.

Acknowledgments This work was in part supported by Hamamatsu Photonics K.K. (Hamamatsu, Japan), the Program for Promotion of Basic Research Activities for Innovative Bioscience, Health and Labor Sciences Research Grants, Research on Psychiatric and Neurological Diseases and Mental Health, and grant-in-aids from the Ministry of Education, Culture, Sport, Science, and Technology, Japan (18700625 awarded to MO and 18390404 to ID). We thank Dr. Lester Clowney for proofreading the manuscript.

References

1. Obrig, H., Villringer, A. 2003. Beyond the visible-imaging the human brain with light. *J. Cereb. Blood Flow Metab.* **23**. 1–18 .
2. Watanabe, E., Maki, A., Kawaguchi, F., Takashiro, K., Yamashita, Y., Koizumi, H., Mayanagi, Y. 1998. Non-invasive assessment of language dominance with near-infrared spectroscopic mapping. *Neurosci. Lett.* **30**. 49–52.
3. Fujiwara, N., Sakatani, K., Katayama, Y., Murata, Y., Hoshino, T., Fukaya, C., Yamamoto, T. 2004. Evoked-cerebral blood oxygenation changes in false-negative activations in BOLD contrast functional MRI of patients with brain tumors. *Neuroimage* **21**. 1464–1471.
4. Watanabe, E., Maki, A., Kawaguchi, Y., Yamashita, Y., Koizumi, H., Mayanagi, Y. 2000. Noninvasive cerebral blood volume measurement during seizures using multichannel near infrared spectroscopic topography. *J. Biomed. Opt.* **5**. 287–290 .
5. Miyai, I., Tanabe, H.C., Sase, I., Eda, H., Oda, I., Konishi, I., Tsunazawa, Y., Suzuki, T., Yanagida, T., Kubota, K. 2001. Cortical mapping of gait in humans: a near-infrared spectroscopic topography study. *Neuroimage* **14**. 1186–1192.
6. Suto, T., Fukuda, M., Ito, M., Uehara, T., Mikuni, M. 2004. Multichannel near-infrared spectroscopy in depression and schizophrenia: cognitive brain activation study. *Biol. Psychiatry* **55**. 501–511.
7. Isobe, K., Kusaka, T., Nagano, K., Okubo, K., Yasuda, S., Kondo, M., Itoh, S., Onishi, S. 2001. Functional imaging of the brain in sedated newborn infants using near infrared topography during passive knee movement. *Neurosci. Lett.* **299**. 221–224.
8. Murata, Y., Katayama, Y., Sakatani, K., Fukaya, C., Kano, T. 2003. Evaluation of extracranial-intracranial arterial bypass function by using near-infrared spectroscopy. *J. Neurosurg.* **99**. 304–310 .
9. Cope, M., Delpy, D.T., Reynolds, E.O., Wray, S., Wyatt, J., van der Zee, P. 1988. Methods of quantitating cerebral near infrared spectroscopy data. *Adv. Exp. Med. Biol.* **222**. 183–189 .
10. Zhao, H., Tanikawa, Y., Gao, F., Onodera, Y., Sassaroli, A., Tanaka, K., Yamada, Y. 2002. Maps of optical differential pathlength factor of human adult forehead, somatosensory motor and occipital regions at multi-wavelengths in NIR. *Phys. Med. Biol.* **47**. 2075–2093.
11. Oda, M., Nakano, T., Suzuki, A., Shimizu, K., Hirano, I., Shimomura, F., Ohmae, E., Suzuki, T., Yamashita, Y. 2000. Nearinfrared time resolved spectroscopy system for tissue oxygenation monitor. *SPIE* **4160**. 204–210.
12. Sakatani, K., Yamashita, D., Yamanaka, T., Oda, M., Yamashita, Y., Hoshino, T., Fujiwara, N., Murata, Y., Katayama, Y. 2006. Changes of cerebral blood oxygenation and optical pathlength during activation and deactivation in the prefrontal cortex measured by time-resolved near infrared spectroscopy. *Life Sci.* **78**. 2734–2741.
13. Zhang, H., Miwa, M., Urakami, T., Yamashita, Y., Tsuchiya, Y. 1998. Simple subtraction method for determining the mean path length traveled by photons in turbid media. *Jpn. J. Appl. Phys.* **37**. 700–704.

14. Patterson, M.S., Chance, B., Wilson, B.C. 1989. Time resolved reflectance and transmittance for the noninvasive measurement of tissue optical properties. *Appl. Opt.* **28**. 2331–2336.
15. Jurcak, V., Tsuzuki, D., Dan, I. 2007. 10/20, 10/10, and 10/5 systems revisited: their validity as relative head-surface-based positioning systems. *Neuroimage* **34**. 1600–1611.
16. Okamoto, M., Dan, I. 2005. Automated cortical projection of head-surface locations for transcranial functional brain mapping. *Neuroimage* **26**. 18–28.